Coke Relocation and Mo Immobilization in Donut-Shaped Mo/HZSM-5 Catalysts for Methane Dehydroaromatization

Ming Cheng, Hugo Cruchade, Ludovic Pinard, Eddy Dib, Honghai Liu, Jiujiang Wang, Xinmei Liu, Zi-Feng Yan, Zhengxing Qin, Svetlana Mintova

ARTICLE

Coke Relocation and Mo Immobilization in Donut-Shaped Mo/HZSM-5 Catalysts for Methane Dehydroaromatization

Ming Cheng[a,†], Hugo Cruchade[b,†], Ludovic Pinard[b], Eddy Dib[b], Honghai Liu[c], Jiujiang Wang[c], Xinmei Liu[a], Zi-Feng Yan[a], Zhengxing Qin[a]*, Svetlana Mintova[b]*

Molybdenum-modified HZSM-5 catalysts are widely used for methane dehydroaromatization (MDA) but suffer from rapid deactivation due to coke formation. The limited diffusion in zeolitic catalysts promotes coke accumulation in micropores, creating concentration gradients of reactants and products within the crystals. In this study, we propose a synthesis approach to evaluate the impact of removing the crystal core in the Mo/HZSM-5 catalyst on the MDA performance. To achieve this, a parent zeolite (Z_P) comprising a silicalite-1 core encased by an HZSM-5 crystal is subjected to two distinct treatments: fluorine (Z_F) and alkaline (Z_{OH}). These treatments dissolve the silicon-rich core, creating a central macropore in the crystals leading to the formation of donuts-shaped catalysts. The alkaline treatment further generates additional mesopores and silanols by leaching atoms from the zeolite framework. The MDA reaction on molybdenum-impregnated zeolite catalysts (Z_P, Z_F, and Z_{OH}) at 973 K was carried out. Interestingly, the "donut"-shaped catalysts modify the nature of the coke deposition, relocating the coke from the micropores to the macropores. Consequently, the removal of the crystal core effectively mitigates catalysts deactivation caused by coke formation. Moreover, the alkaline-treated catalyst exhibits additional beneficial properties, such as increased silanols and higher surface area, which help to limit the sintering of molybdenum carbides during the MDA reaction. The new strategy improves the performance and stability of Mo/HZSM-5 catalysts in methane dehydroaromatization.

1. Introduction

Methane dehydroaromatization under non-oxidative conditions (MDA: $6CH_4 \rightleftarrows C_6H_6 + 9H_2$) over bifunctional Mo/HZSM-5 catalysts has raised the hope of the scientific community over the last decades as a new potential energy source.[1] Indeed, MDA allows hydrogen production while capturing the carbon from methane by forming valuable petrochemical products (*e.g.* aromatics). Therefore, it appears as a more sustainable alternative to energy production through natural gas and biogas combustion. However, the challenging conditions of MDA, the diverse presence of molybdenum and carbon species, and their constant evolution throughout the reaction pose significant difficulties in elucidating the underlying mechanisms.[2,3] Hence, the industrial development of MDA is still impeded by (i) a relatively low benzene yield, limited by thermodynamics at about 12.5% (700 °C), and (ii) a rapid catalyst deactivation due to coke formation.[4,5] Catalyst development is one of the strategies identified to address such challenges.[3,6]

Different ways of catalysts improvement have been reported, such as Mo/Al balance tuning[7–9], variation of molybdenum loading approach[10,11], pretreatment[12–14], metallic promoter addition[15–17], or crystal engineering[18–21]. The latter represents an extensive research topic for hydrocarbon processing catalyzed by acidic-microporous materials since the diffusional limits in zeolites lead to coke accumulation and mitigate the efficiency of the crystal core.[22] In this sense, the decrease of the diffusion pathway in MDA catalysts has been studied through hierarchization and crystal nanosizing.[18,19,23] The shortening of the crystal size favors the desorption of the products but enhances the molybdenum carbides migration on the external surface. On the contrary, a long diffusional pathway enhances the condensation of products within the micropores but mitigates the sintering of molybdenum carbides. Therefore, certain nanosized Mo/HZSM-5 does not show higher stability than micron-sized catalysts. Thus, diffusion in MDA catalysts is crucial, challenged by the dual mode of deactivation governing MDA involves the molybdenum sintering and coke deposition.

Hollow type zeolites can be considered as intermediates between the micron-sized zeolites (*i.e.* high diffusion pathway and low external surface) and nanosized zeolites (*i.e.* low diffusion pathway and high external surface). They show an extended lifetime compared to commercial HZSM-5.[24–26] The variable wall thickness of the hollow type zeolites may enhance diffusion and help inhibiting coke deposition. As an intermediate material a crystal with a big central hole can be considered. A selective dissolution of silicon-rich part of silicalite-1-Core/HZSM-5-Shell material or HZSM-5 zeolites synthesized by the seed-assisted method through post-treatments has been reported.[20,27] Core/shell materials made with silicalite-1 and HZSM-5 allow tuning of catalysts reactivity. The diffusion pathway is not shortened, but the absence of

Brønsted acid sites in the silicalite-1 part reduced the probability of further transforming the products into heavier compounds. An acidic (NH_4F) or alkaline (NaOH) treatment of zeolite catalysts may dissolve the silicon-rich core of the crystals. Moreover, the nature of the post-treatment can modify the textural and chemical properties of the catalysts.[28–30]

This study reports how reducing diffusion pathways by removing the crystal core affects catalysts behavior during methane dehydroaromatization (MDA). To achieve this, a novel synthesis strategy was developed to create coreless Mo/HZSM-5, named donut-shaped catalysts. Fluorine and alkaline post-treatments were applied to the silicalite-1-Core/HZSM-5-Shell material to selectively dissolve its core. The textural and chemical properties of the fresh catalysts were characterized and their catalytic performance in MDA was evaluated. Furthermore, catalyst deactivation and coking mechanisms were explored through post-reaction characterization. This comprehensive approach provides insights into the role of the crystal core in the MDA process and its impact on catalyst performance.

2. Experimental

2.1. Materials synthesis

The reagents used for the preparation of ZSM-5 zeolite are Tetraethyl orthosilicate (TEOS, 28.8 % calculated as SiO_2), Tetrapropylammonium hydroxide (TPAOH, 25% w/w aqueous solution, AR), Aluminum sulfate ($Al_2(SO_4)_3{\cdot}18H_2O$, AR), Sodium hydroxide (NaOH, Granular, AR), Tetrapropylammonium bromide (TPABr, AR), Ammonium fluoride (NH_4F, AR), Ammonium Chloride (NH_4Cl, AR), Ammonium molybdate ($(NH_4)_6Mo_7O_{24}{\cdot}4H_2O$, AR). All chemicals were purchased from Sinopharm Chemical Reagent Corporation and used directly without further purification.

2.1.1. Silicalite-1 seeds

Silicalite-1 was synthesized to be used as seeds for the crystallization of the parent zeolite (Z_P). An aqueous suspension of TPAOH and TEOS resulting in a precursor suspension with a molar composition of 0.35 TPAOH : 1 SiO_2 : 19 H_2O was prepared and stirred at room temperature for 12 h. Then, the suspension was hydrothermally treated at 373 K for 24 h in a polypropylene bottle. The solid was collected after cycles of centrifugation and washing with ultrapure water until reaching a pH value of the supernatant of 7.

2.1.2. Parent zeolite (sample Z_P).

The parent zeolite was synthesized from a gel with a molar composition of 0.033 Al_2O_3 : 1.0 SiO_2 : 0.13 TPABr : 0.56 NH_4F : 23.13 H_2O. First, an aqueous suspension of $Al_2(SO_4)_3{\cdot}18H_2O$ and TPABr was prepared in a polypropylene bottle and kept under stirring at room temperature for 30 min. Then, TEOS was added, and the resulting gel was kept under stirring at ambient temperature overnight. The silicalite-1 seeds synthesized (see the procedure above) were added to reach 15 wt.% of the total silica source of the gel. After 2 h of stirring, NH_4F and water were added, and the gel was kept under stirring for 2 h. The mixture was hydrothermally treated in a Teflon-lined stainless-steel autoclave for 3 days at 373 K. The solid product was recovered after successive centrifugation and washing with ultrapure water until reaching a pH value of the supernatant of 7. Then, the product was dried at 353 K for 10 h and calcinated at 823 K under static air for 12 h with a ramp of 2 K min^{-1}.

2.2. Donut-shaped zeolite catalysts

2.2.1. Donut-shaped zeolite catalysts prepared by fluorine treatment (Z_F).

The Z_F sample was prepared by mixing the Z_P with an aqueous solution of NH_4F (40 wt.%) with a solid/liquid ratio of 1 : 20. The mixture was kept under stirring for 1 h at 323 K. Then the product was separated by centrifugation, washed with deionized water, and dried at 353 K overnight and calcined at 823 K in static air for 12 h with a ramp of 2 K min^{-1}.

2.2.2. Donut-shaped zeolite catalysts prepared by alkaline treatment (Z_{OH}).

The Z_{OH} sample was prepared by mixing the Z_P with an aqueous solution of NaOH at 0.2 mol L^{-1} with a solid/liquid ratio of 1 : 30. The mixture was kept under stirring for 0.5 h at 353 K. The treated zeolite was separated by centrifugation, washed with deionized water, and dried at 353 K overnight. The dried sample was NH_4^+-exchanged three times with an NH_4Cl solution (1 mol L^{-1}) at 358 K for 3 h under stirring using a solid/liquid ratio of 1 : 30. Then, the sample was washed with deionized water, dried at 353 K overnight and calcinated at 823 K in static air for 12 h with a ramp of 2 K min^{-1}.

2.2.3. Molybdenum impregnation of parent (Z_P) and donut-shaped (Z_F and Z_{OH}) catalysts

The parent (Z_P) and donut-shaped samples (Z_F and Z_{OH}) were wet impregnated with molybdenum. 2 g of the zeolite sample was mixed with an aqueous solution containing 0.147 g of $(NH_4)_6Mo_7O_{24}{\cdot}4H_2O$ and 1.6 mL of ultra-pure water. Then, the samples were calcined at 823 K in static air for 4 h with a ramp of 2 K min^{-1}. The molybdenum impregnated samples were denoted [Mo]-Z_P, [Mo]-Z_F and [Mo]-Z_{OH}.

2.3. Characterization

The X-ray diffraction (XRD) patterns of the zeolite samples were collected from 3 to 50° on a Bruker D8 Advance diffractometer equipped with Cu and K_α radiation (λ = 1.5418 Å) at 40 kV and the scanning speed 0.8° min^{-1}.

The porosity of zeolite samples was analyzed on a 3Flex Micromeretics instrument at 77 K. Before the measurement, the samples were degassed at 573 K under vacuum for 4 h. BJH model was applied to the adsorption branch of the isotherms to evaluate the pore size distribution (PSD). The specific surface area was determined using BET method, and the micropore volume and external surface area from the t-plot method.

The morphology of the samples was determined using a JSM-7900F JEOL scanning electron microscope (SEM) equipped with

a field emission gun. The acceleration voltage, beam current and work distance were 4 kV, 2 nA, and 10 mm, respectively. Transmission electron microscopy (TEM) study was performed on a JEM-2100 JEOL microscope with an acceleration voltage of 200 kV.

The Si/Al ratio of samples was determined based on ^{29}Si NMR spectroscopy; the spectra were acquired at 12 kHz. Additionally, ^{1}H NMR spectra of the zeolite samples using a 11.7 T Bruker Avance 500 spectrometer at 40 kHz were collected. Prior to the ^{1}H NMR measurements, the samples were degassed at 573 K for 4 h, and kept in Ar atmosphere.

The molybdenum content was measured by Inductively coupled plasma mass spectrometry (ICP-MS) on a 7900 ICP-MS (Agilent) device.

The Fourier transform infrared spectroscopy (FTIR) characterization of samples was performed on a NEXUS Series (Nicolet) spectrometer at 4 cm^{-1} optical resolution. Prior to IR measurements, the zeolites were pressed into self-supporting discs (~20 mg) and pretreated in the IR cell attached to a vacuum line (10^{-6} Torr) at 823 K (3.5 K·min^{-1}) for 4 h. Then the adsorption of pyridine was performed at 423 K until an adsorption equilibrium was reached, then the cell was evacuated at 523 K in order to remove the physisorbed species. All spectra were normalized to 20 mg zeolite sample (self-supported wafer). The amount of pyridine adsorbed on Brønsted and Lewis sites at different temperatures was determined using the integrated area of the bands at 1540 cm^{-1} and 1490 cm^{-1}, respectively. The extinction coefficients used in this study were ε (B) 1545 = 1.02 cm mol^{-1} and ε (L) 1454 = 0.89 cm mol^{-1}.[27,31]

2.4. Catalytic test

Methane dehydroaromatization (MDA) reaction was performed on molybdenum containing samples in a fixed bed reactor at atmospheric pressure and 973 K. 0.5 g of catalyst with particles size in the range of 0.25 - 0.5 mm were packed in a quartz tube reactor (7 mm internal diameter). Prior to the reaction, the catalyst was heated from room temperature to 973 K with a heating rate of 5 K min^{-1} under an argon flow of 15 ml min^{-1}. MDA reaction was carried out at a WHSV of 1.2 h^{-1} with a feed gas mixture of 90 vol.% CH_4 and 10 vol.% N_2. The gas composition at the reactor outlet was characterized by online gas chromatography (Chromatec, Crystal 9000) using nitrogen as an internal standard.

2.5. Characterization of spent catalysts

After 10 h of reaction, the spent catalysts were recovered and characterized, and the samples were named [Mo]-$Z_{P\text{-}Spent}$, [Mo]-$Z_{F\text{-}Spent}$ and [Mo]-$Z_{OH\text{-}Spent}$. The coke content on the spent catalysts was measured by thermogravimetric analysis on a SETSYS (SETERAM, Caluire, France) thermobalance. The samples were heated in an alumina crucible from room temperature to 1273 K at a heating rate of 10 K min^{-1} under a flow of air of 40 ml min^{-1}.

The pore volume of the spent catalysts was determined by N_2 adsorption at 77 K using a Micromeretics 3Flex device. The samples were degassed at ambient temperature for 4 h.

3. Results and discussions

3.1. Material synthesis and characterization

3.1.1. Z_P zeolite sample

To study the impact of zeolite crystal core removal on MDA performance, donut-shaped zeolite samples were prepared by a post-synthetic treatment of the parent ZSM-5 zeolite sample (Z_P). The Z_P was synthesized using aluminum-containing gel through the seed-assisted method in fluoride media. The silicalite-1 used as seeds were prepared with a particle size of about 80 nm (**Figure 1**) and a high crystallinity (**Figure SI. 1**).

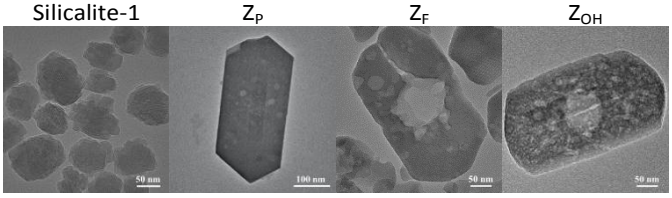

Figure 1. Transmission electron microscopy images of silicalite-1 seeds, Z_P, Z_F and Z_{OH} zeolite samples.

The silicalite-1 crystals act as seeds providing surfaces for the growth of the zeolite crystals[32] and control the crystallization kinetics of the ZSM-5 phase in fluoride media[27]. The resulting material has a pure MFI framework structure (**Figure SI. 2**) and depicts a coffin shape morphology with a crystal size of about 350 nm (**Figure 1**).

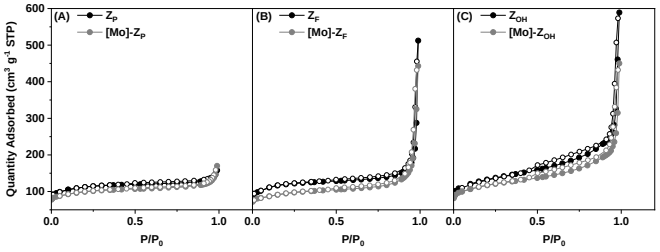

Figure 2. Nitrogen adsorption/desorption isotherms of parent Z_P (A), Z_F (B), and Z_{OH} (C) (black circles) and molybdenum-impregnated [Mo]-Z_P, [Mo]-Z_F and [Mo]-Z_{OH} (grey circles) zeolite samples.

The Z_P sample was characterized by nitrogen physisorption and the isotherm is presented in **Figure 2**. The micropore and total pore volume of 0.16 cm^3 g^{-1} and 0.21 cm^3 g^{-1}, respectively for the Z_P sample are measured (**Table 1**). Further the hydrophobicity of the sample was measured by FTIR; the IR spectra of samples in the 3800-3400 cm^{-1} region are depicted in **Figure 3 A.**

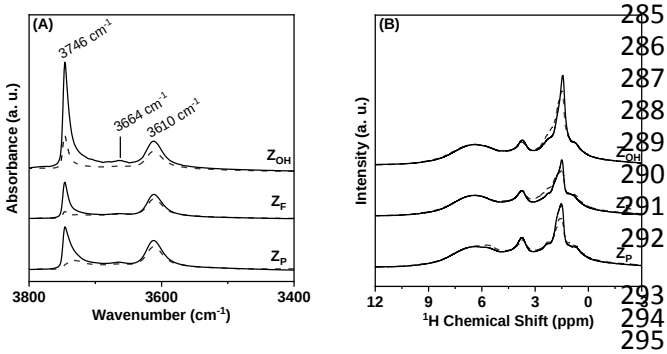

Figure 3. Infrared spectra (A) in the ν(OH) region of 3800-3400 cm^{-1} and ^{1}H NMR spectra (B) of parent Z_P, Z_F, and Z_{OH} (solid line) and molybdenum-impregnated [Mo]-Z_P, [Mo]-Z_F and [Mo]-Z_{OH} (dashed line) zeolite samples.

The peak at 3610 cm^{-1} corresponds to bridged hydroxyls present in the Z_P sample. Despite the large crystal size, the Z_P contains isolated silanols confirmed by the presence of a band at 3746 cm^{-1}.[33] ^{1}H NMR spectra (**Figure 3 B)** reveal the non-H-bonded silanols, *i.e.* isolated silanols appearing at 1 -3 ppm and Brønsted acid sites appearing at 4 ppm.[34,35] These silanols possibly localized within the crystal core are due to the presence of silicalite-1 nanocrystal core.[34,36,37] The Z_P sample exhibits a heterogeneity with a silicon-rich core surrounded by an aluminum-rich shell. The Si/Al ratio of the Z_P sample is 38 (**Table 2**), corresponding to a theoretical aluminum concentration of 405 µmol g^{-1}. However, the Brønsted acid site concentration measured by pyridine adsorption using IR spectroscopy is lower (**Table 2**) that may be due to the presence of extra-framework aluminum (**Figure 3 A**, peak at 3664 cm^{-1}) resulting in Lewis acidity (**Table 2**).

Table 1. Textural properties of the parent Z_P, Z_F, and Z_{OH} and molybdenum-impregnated [Mo]-Z_P, [Mo]-Z_F and [Mo]-Z_{OH} zeolite samples.

Sample	S_{Ext}[a] $m^2 g^{-1}$	V_{Micro}[a] $cm^3 g^{-1}$	V_{Tot}[b] $cm^3 g^{-1}$
Z_P	30	0.16	0.32
[Mo]-Z_P	29	0.15	0.26
Z_F	47	0.17	0.79
[Mo]-Z_F	47	0.13	0.68
Z_{OH}	180	0.13	0.91
[Mo]-Z_{OH}	132	0.12	0.69

[a]t-plot, [b]volume adsorbed at P/P_0= 0.99.

3.1.2. Z_F and Z_{OH} donut-shaped zeolite samples

The post-treatment of the parent zeolite in fluoride (sample Z_F) and alkaline (sample Z_{OH}) media resulted in donut-shaped materials (**Figure 1**) while preserving the high crystallinity and MFI type framework structure (**Figure SI. 2**). Both Z_F and Z_{OH} zeolite samples keep the coffin shape morphology of the parent Z_P and feature a central hole with a diameter corresponding to the size of the silicalite-1 seeds (≈ 80 nm). The macropores formed in both samples due to the removal of the silicalite-1 seeds increase the total pore volume and the external surface without impacting the micropore volume (**Table 1**). The decrease of the Si/Al ratio after treatments confirms the removal of the silicon-rich part of the zeolite crystals (**Table 2**). The removal of the seeds results in a partial breaking of the zeolite crystals (**Figure SI. 3**).

In the case of the fluoride treatment, the removal of silicalite-1 results in a lower amount of silanols of sample Z_F in comparison to the parent sample Z_P (**Figure 3**). On the contrary, the alkaline leaching extracts part of the framework atoms, creating additional intracrystalline mesopores (**Figure SI. 4**) and additional silanols defects (**Figure 3**).

Table 2. Chemical composition and acidity of parent Z_P, Z_F, and Z_{OH} and molybdenum-impregnated [Mo]-Z_P, [Mo]-Z_F and [Mo]-Z_{OH} samples.

Sample	$(Si/Al)_{Framework}$[a]	[Mo][b] wt.%	$[H^+]$[c] µmol g^{-1}	[L][c] µmol g^{-1}
Z_P	38.1	/	276	108
[Mo]-Z_P	36.1	3.2	228	151
Z_F	34.5	/	245	44
[Mo]-Z_F	32.3	3.3	221	141
Z_{OH}	26.5	/	226	188
[Mo]-Z_{OH}	27.0	3.2	200	210

[a]determined by solid-state ^{29}Si MAS NMR, [b]determined by ICP-MAS, [c]Brønsted ($[H^+]$) and Lewis ([L]) acid sites quantified by pyridine desorption at 423 K by FTIR.

3.1.3. Mo-impregnated zeolite samples: [Mo]-Z_P, [Mo]-Z_F and [Mo]-Z_{OH}

The three zeolite samples (Z_P, Z_F and Z_{OH}) were wet-impregnated with about 3 wt.% of molybdenum (**Table 2)**. **Figure 3 A** depicts the OH region of the IR spectra for samples before and after Mo impregnations. On the three samples, the intensity of the bridged hydroxyls band decreases after molybdenum loading. Indeed, during the calcination a part of the molybdenum migrates within the micropores and reacts with the framework aluminum.[38] The quantity of molybdenum anchored to the framework aluminum ($[Mo]_{Anch}$) can be estimated from the loss of Brønsted acid sites as determined by pyridine adsorption using IR of samples before and after Mo loading (**Table 2**). Assuming a stoichiometry of one molybdenum atom per aluminum atom[39,40], the $[Mo]_{Anch}$ is estimated to be of 0.4 wt.% and only a half of this value on [Mo]-Z_F and [Mo]-Z_{OH} samples (**Table 2**). In both IR and ^{1}H NMR spectra (**Figure 3**), the intensity of the isolated silanols bands decreases after Mo loading on the 3 samples ([Mo]-Z_P, [Mo]-Z_F and [Mo]-Z_{OH}). Thus, part of the molybdenum is anchored to the zeolite framework on the three samples by interacting with the isolated silanols. Mo-mapping of the samples [Mo]-Z_P, [Mo]-Z_F and [Mo]-Z_{OH} by EDS reveal the homogeneous dispersion of molybdenum located within the crystals volume and on the surface (**Figure 4),** except in the empty core on [Mo]-Z_F and [Mo]-Z_{OH}**.**

Based on the characterization results presented above, the samples can be described as follow: (i) [Mo]-Z_P as silicon-core /ZSM-5-shell material, (ii) [Mo]-Z_F as ZSM-5 zeolite with macropores created by seed core removal, and (iii) [Mo]-Z_{OH} as ZSM-5 zeolite with high external surface and macropores created by seed core removal with intracrystalline mesopores and additional external silanols.

Both post-treatments of the zeolites in OH^- and F^- media decrease the number of Brønsted acid sites, hence, the molybdenum anchored to BAS ($[Mo]_{Anch}$).

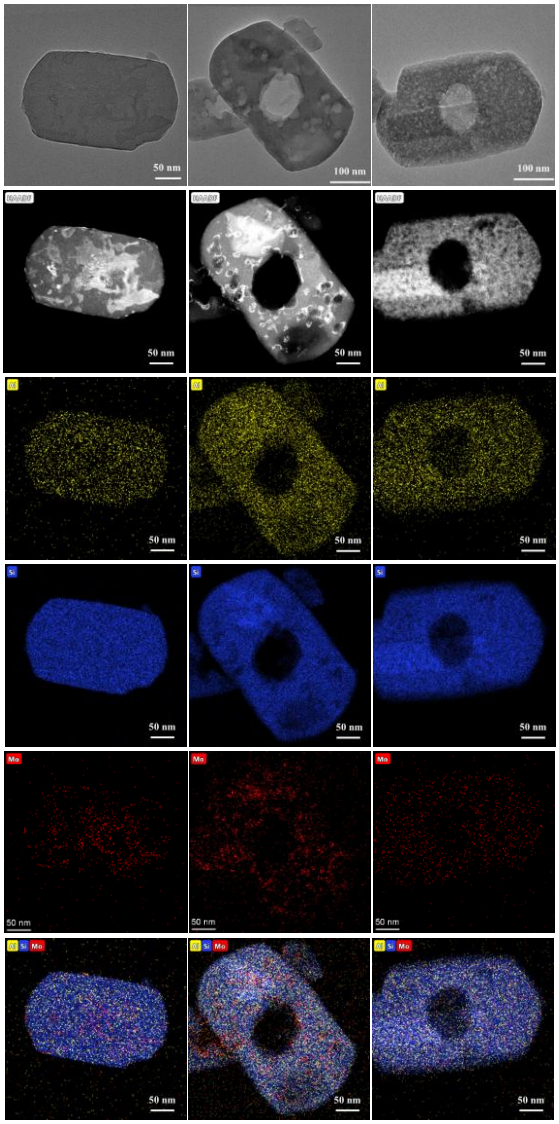

Figure 4. TEM and EDS mapping of [Mo]-Z_P (left), [Mo]-Z_F (middle) and [Mo]-Z_{OH} (right) zeolite samples.

3.2. Catalytic evaluation of zeolite catalysts in MDA reaction

Methane dehydroaromatization was carried out on parent [Mo]-Z_P and donut-shaped [Mo]-Z_F, [Mo]-Z_{OH} zeolite catalysts at 973 K.

3.2.1. MDA on [Mo]-Z_P parent zeolite catalyst

The methane consumption rate on the [Mo]-Z_P catalyst sharply decreases with the time on stream, following the same behavior as Mo/ZSM-5 catalysts with similar Mo content and Si/Al ratio, previously reported in the literature[7] (**Figure SI. 5**). The gain and loss in methane consumption (**Figure 5 A**), benzene production (**Figure 5 B**), and the deactivation rate constant (k_d) calculated assuming a first-order law[7] (**Figure 5 C**) over 10 h reaction using the three catalysts are presented. The methane consumption on the [Mo]-Z_P catalyst (31 mmol $g_{Cat.}^{-1}$, **Figure 5 A**) and the k_d value (0.14 h^{-1}) are in the same order of magnitude as reported in the literature[7,9].

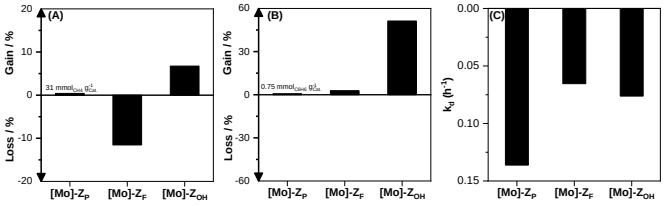

Figure 5. Impact of fluorine ([Mo]-Z_F) and alkaline treatment ([Mo]-Z_{OH}) relative to the parent zeolite ([Mo]-Z_P) on (A) the CH_4 consumption and (B) the benzene formation on time on stream window of 10 h, and (C) benzene first order deactivation rate (k_d).

The analysis of coke on the spent [Mo]-$Z_{P\text{-}Spent}$ catalyst was carried out by thermogravimetry and the content of soft coke and hard coke at combustion temperatures of 722 and 846 K, respectively were measured (**Figure 6**)[38,41].

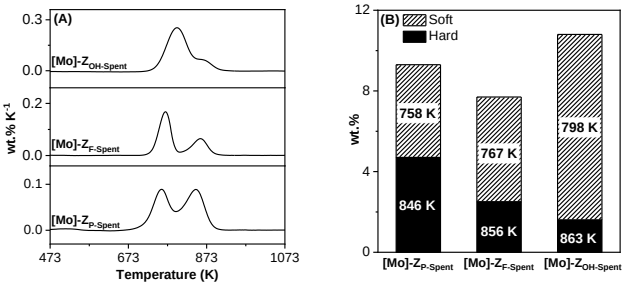

Figure 6. Coke on the spent catalysts ([Mo]-$Z_{P\text{-}Spent}$ [Mo]-$Z_{OH\text{-}Spent}$ and [Mo]-$Z_{F\text{-}Spent}$) after 10 h of reaction represented by derivative curves of thermogravimetric measurements (A) and content of soft coke and hard coke and combustion temperatures determined by thermogravimetric analysis (B).

The change in the micropore volume measured by N_2 adsorption (**Figure 7 A**), is a deactivation descriptor.[42] Indeed, Hensen *et al.* showed a linear dependence between the coke content and the remaining microporous volume of zeolite catalysts. For the [Mo]-$Z_{P\text{-}Spent}$ catalyst, a loss of half of the initial microporous volume corresponding to a total coke content of 9.3 wt.% was measured (**Figure 6 B and Figure 7 A**). Moreover, the mesopore volume of the [Mo]-$Z_{P\text{-}Spent}$ catalyst remains almost unchanged (**Figure 7 A**), thus one can conclude that the coke is mainly located in the microporous volume (**Figure 7 B**). The deactivation of the [Mo]-$Z_{P\text{-}Spent}$ catalyst during MDA also occurs through molybdenum carbides sintering located on the external surface (**Figure 8**). Such clusters are mostly localized on the ZSM-5 part of the [Mo]-$Z_{P\text{-}Spent}$ catalyst, while Mo species seems to have a better dispersion on the silicalite-1 core.

The methane consumption, k_d, and combustion temperatures of soft coke and hard coke, and remaining microporous volume of the parent [Mo]-Z_P catalyst are similar to the ones reported for ZSM-5 zeolite earlier[6,9,38,42]. Thus, the parent sample [Mo]-Z_P can be considered as a reliable reference in order to understand the behavior of the donut-shaped zeolite catalysts in the MDA reaction.

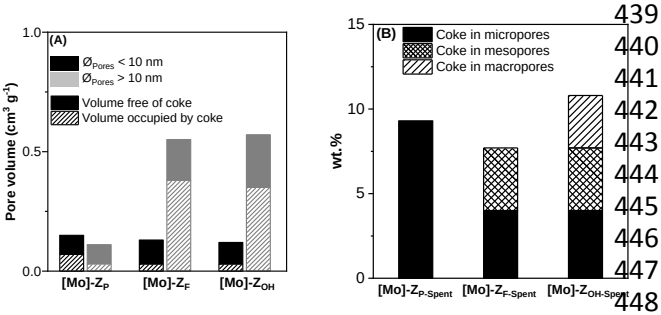

Figure 7. Characterization of [Mo] $Z_{P\text{-}Spent}$, [Mo]$Z_{F\text{-}Spent}$ and [Mo]$Z_{OH\text{-}Spent}$ catalysts after 10 h of reaction: pore volume with and without coke, measured by nitrogen sorption (A) and coke distribution in different pores of zeolite catalysts (B).

3.2.2. MDA on [Mo]-Z_F and [Mo]-Z_{OH} donut-shaped catalysts

The methane consumption on the [Mo]-Z_F catalyst decreases slightly without any change in benzene production (**Figure 5 A and B**). The NH_4F etching used for the preparation of [Mo]-Z_F leads to a lower amount of $[Mo]_{Anch}$ (see section 3.1.3), considered as a precursor for MDA actives sites[9], thus lowering the methane consumption. However, the presence of the central hole enhances the catalyst stability, probably by mitigating the coke deposit within zeolite micropores (**Figure 5 C and Figure SI. 6**). A loss of 0.03 $cm^3\ g^{-1}$ of the micropore volume (V_{Micro}) of sample [Mo]-$Z_{F\text{-}Spent}$ shown by the black column (volume occupied by coke) is depicted in **Figure 7 A**. Based on the linear relationship presented elsewhere[42], a coke content of 4.0 wt.% located in the micropore volume of this sample is calculated. The total coke content of [Mo]-$Z_{F\text{-}Spent}$ measured by TG is 7.7 wt.% (**Figure 6**) and based on the coke balance, 3.7 wt.% of the coke is located in the macropores (more details on the calculation can be found in the supporting information) due to the presence of a hole in the donut-shaped structure (**Figure 7 A**). After 10 h of MDA, molybdenum carbide was formed and predominantly deposited on the external surface of the catalysts.

The alkaline treatment of the parent zeolite substantially improves methane consumption and benzene production as shown in **Figure 5 A and B**. The higher activity is probably not due to a higher molybdenum-aluminum anchoring since for both samples, [Mo]-Z_{OH} and [Mo]-Z_F, a similar $[Mo]_{Anch}$ is measured. Despite the decrease in the number of active sites of sample [Mo]-Z_{OH} compared to [Mo]-Z_P, the activity gain may result from additional small mesopores connected to the micropore network and better stability of molybdenum carbides present (**Figure 8**). This can be explained with the high external surface of sample [Mo]-Z_{OH} in comparison to the parent [Mo]-Z_P and [Mo]-Z_F catalysts (**Table 1**). Moreover, the [Mo]-Z_{OH} contains silanols defects that interact with molybdenum and prevent sintering of molybdenum carbides during the MDA reaction.

The deactivation rate constant (k_d) remains similar for the [Mo]-Z_{OH} sample regardless of the post-treatment procedure applied (**Figure 5 C and Figure SI. 6**). The additional small mesopore network has no impact on the catalyst stability, thus the mitigation of deactivation is only due to the dissolution of the silicalite-1 seeds resulting in a decrease of the diffusion pathway within the [Mo]-Z_{OH} crystals. For the spent [Mo]-$Z_{F\text{-}Spent}$ and [Mo]-$Z_{OH\text{-}Spent}$ donut-shaped catalysts, the losses of V_{Micro} and V_{Tot} are similar no matter the post-treatment applied (**Figure 7 A**). Yet, the total coke content is higher on the [Mo]-$Z_{OH\text{-}Spent}$ catalyst than on the [Mo]-$Z_{F\text{-}Spent}$ free of silanols defects (**Figure 6**). The presence of a hole leads to better accessibility of oxygen to coke during TGA measurements. Thus, a higher amount of soft coke was measured on [Mo]-$Z_{F\text{-}Spent}$ and [Mo]-$Z_{OH\text{-}Spent}$ catalysts (**Figure 6**). Moreover, the presence of mesopores in the [Mo]-Z_{OH} catalyst enhances this phenomenon. A similar shift was previously reported on mesoporous catalysts[19]. The location of coke in the [Mo]-$Z_{OH\text{-}Spent}$ catalysts can be estimated as follow (more details on the calculation can be found in the supporting information): (i) 4.0 wt.% in the micropores, (ii) 3.7 wt.% in macropores, and (iii) by coke balance 3.1 wt.% in the additional mesopores (**Figure 7 B**). The coke retention in the mesopores can be explained with the presence of silanols known to act as coke trap[43–45]. Thus, the retention of soft coke in sample [Mo]-$Z_{OH\text{-}Spent}$ is enhanced (**Figure 6**)[19]. Only the coke deposited in the micropores of the [Mo]-$Z_{OH\text{-}Spent}$ deactivates the catalyst. The coke in the different pores of the [Mo]-$Z_{OH\text{-}Spent}$ catalyst does not directly affect the loss of free total pore volume regarding the [Mo]-$Z_{F\text{-}Spent}$ catalyst, as exemplified in **Figure 7 B**. Yet the soft coke and hard coke combustion occur at higher temperatures (**Figure 6**), despite the presence of mesopores allowing higher accessibility to oxygen[18,42].

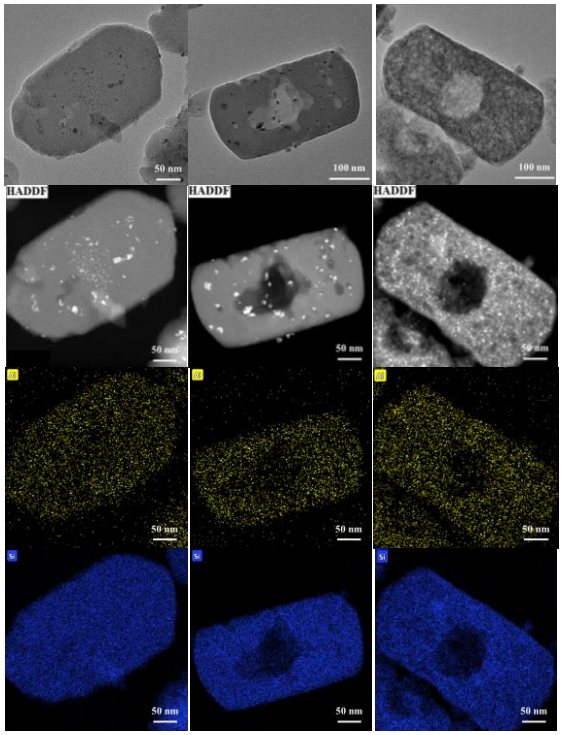

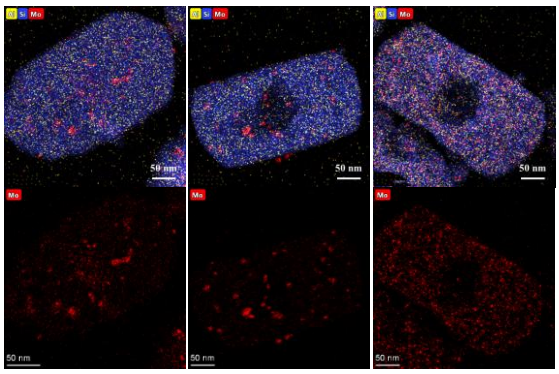

Figure 8. TEM and EDS mapping images of [Mo] $Z_{P\text{-}Spent}$ (left), [Mo]$Z_{F\text{-}Spent}$ (middle) and [Mo]$Z_{OH\text{-}Spent}$ (right) catalysts after 10 h of reaction.

4. Conclusions

The synthesis of donut-shaped catalysts containing molybdenum was successfully carried out by NH_4F and NaOH post-treatment of silicalite-1-core/HZSM5-shell zeolite composites. Both treatments dissolve the silicon-rich core of the parent silicalite-1-core/HZSM5 sample and the total porosity changed in the order: [Mo]-Z_P < [Mo]-Z_F < [Mo]-Z_{OH}. Both treatments of the parent silicalite-1-core/HZSM5 sample (Z_p) resulted in donut-shaped catalysts however the [Mo]-Z_{OH} contains higher amount mesopores and isolated silanols. The catalytic test of the three samples in MDA reaction revealed deposition of coke in the micropores of the catalysts. While in the donut-shaped catalysts, the decrease of the diffusion pathway improves the stability of the catalysts during MDA by shifting the coke location from micropores to macropores. Extra coke deposits in the mesopores of the alkaline-treated catalyst ([Mo]-Z_{OH}) was found but without impacting its deactivation. Moreover, the presence of silanols and the high external surface of the [Mo]-Z_{OH} catalyst mitigate the sintering of molybdenum carbides and lead to higher activity in the MDA reaction.

5. Conflicts of interest

There are no conflicts to declare.

6. Acknowledgements

We acknowledge the financial support from the National Natural Science Foundation of China (22178389) and PetroChina (KYWX-21-021, PRIKY21084). The financial support from Industrial Chair “EcoGas”, TotalEnergies and the Region Normandie is acknowledged too. Co-funded by the European Union (ERC, ZEOLIghT, 101054004). Views and opinions expressed are however those of the author(s) only and do not necessarily reflect those of the European Union or the European Research Council. Neither the European Union nor the granting authority can be held responsible for them. The support of the Centre for Zeolites and Nanoporous Materials Label of Excellence, Normandy Region (CLEAR) is acknowledged.

7. References

1 N. Elrefaei, N. Basha, M. Nounou, H. Nounou, A. Ashok and M. Al-Rawashdeh, *ChemCatChem*, 2022, **14**, e202200711.
2 I. Vollmer, I. Yarulina, F. Kapteijn and J. Gascon, *ChemCatChem*, 2019, **11**, 39–52.
3 N. Kosinov and E. J. M. Hensen, *Adv. Mater.*, 2020, **32**, 2002565.
4 U. Menon, M. Rahman and S. J. Khatib, *Appl. Catal. A: Gen.*, 2020, **608**, 117870.
5 P. Moghimpour Bijani, M. Sohrabi and S. Sahebdelfar, *Chem. Eng. Technol.*, 2012, **35**, 1825–1832.
6 H. Cruchade, I. C. Medeiros-Costa, N. Nesterenko, J.-P. Gilson, L. Pinard, A. Beuque and S. Mintova, *ACS Catal.*, 2022, **12**, 14533–14558.
7 M. Rahman, A. Infantes-Molina, A. S. Hoffman, S. R. Bare, K. L. Emerson and S. J. Khatib, *Fuel*, 2020, **278**, 118290.
8 K. Zhao, L. Jia, J. Wang, B. Hou and D. Li, *New J. Chem.*, 2019, **43**, 4130–4136.
9 A. Beuque, H. Hu, E. Berrier, A. Sachse, J.-F. Paul and L. Pinard, *Catalysis Today*, , DOI:10.1016/j.cattod.2022.06.001.
10 S. V. Konnov, F. Dubray, E. B. Clatworthy, C. Kouvatas, J.-P. Gilson, J.-P. Dath, D. Minoux, C. Aquino, V. Valtchev, S. Moldovan, S. Koneti, N. Nesterenko and S. Mintova, *Angew. Chem. Int. Ed.*, 2020, **59**, 19553–19560.
11 M. T. Portilla, F. J. Llopis, M. Moliner and C. Martinez, *Appl. Sci.*, 2021, **11**, 5465.
12 P. Tan, *Catal. Commun.*, 2018, **103**, 101–104.
13 A. Sridhar, M. Rahman, A. Infantes-Molina, B. J. Wylie, C. G. Borcik and S. J. Khatib, *Appl. Catal. A: Gen.*, 2020, **589**, 117247.
14 C. H. L. Tempelman, X. Zhu and E. J. M. Hensen, *Chin. J. Catal.*, 2015, **36**, 829–837.
15 P. D. Sily, F. B. Noronha and F. B. Passos, *J. Nat. Gas Chem.*, 2006, **15**, 82–86.
16 T. E. Tshabalala, N. J. Coville and M. S. Scurrell, *Appl. Catal. A: Gen.*, 2014, **485**, 238–244.
17 S. Burns, J. S. J. Hargreaves, P. Pal, K. M. Parida and S. Parija, *Catal. Today*, 2006, **114**, 383–387.
18 K. Liu, M. Çağlayan, A. Dikhtiarenko, X. Zhang, O. Sayidov, E. Abou-Hamad, J. Gascon and A. Dutta Chowdhury, *Catalysis Today*, 2023, **408**, 22–35.
19 C. H. L. Tempelman, V. O. de Rodrigues, E. R. H. van Eck, P. C. M. M. Magusin and E. J. M. Hensen, *Microporous Mesoporous Mater.*, 2015, **203**, 259–273.
20 D.-Y. Hong, H. S. Kim, H. Zhang, S. K. Kang, E. T. Tikue and P. S. Lee, *Crystals*, 2021, **11**, 647.
21 Y. Wu, L. Emdadi, S. C. Oh, M. Sakbodin and D. Liu, *J. Catal.*, 2015, **323**, 100–111.
22 C. H. Christensen, K. Johannsen, E. Törnqvist, I. Schmidt, H. Topsøe and C. H. Christensen, *Catal. Today*, 2007, **128**, 117–122.
23 W. Zhang, D. Ma, X. Han, X. Liu, X. Bao, X. Guo and X. Wang, *Journal of Catalysis*, 1999, **188**, 393–402.
24 M. Huang, J. Li, Q. Liu, M. Zhang, Z. Liu and B. Gao, *Fuel*, 2023, **334**, 126765.
25 X. Huang, X. Jiao, M. Lin, K. Wang, L. Jia, B. Hou and D. Li, *Catal. Sci. Technol.*, 2018, **8**, 5740–5749.
26 P. Zhu, G. Yang, J. Sun, R. Fan, P. Zhang, Y. Yoneyama and N. Tsubaki, *J. Mater. Chem.*, 2017, **5**, 8599–8607.

27 Z. Qin, L. Lakiss, L. Tosheva, J.-P. Gilson, A. Vicente, C. Fernandez and V. Valtchev, *Adv. Funct. Mater.*, 2014, **24**, 257–264.

28 Z. Qin, L. Pinard, M. A. Benghalem, T. J. Daou, G. Melinte, O. Ersen, S. Asahina, J.-P. Gilson and V. Valtchev, *Chem. Mater.*, 2019, **31**, 4639–4648.

29 J. C. Groen, L. A. A. Peffer, J. A. Moulijn and J. Pérez-Ramírez, in *Studies in Surface Science and Catalysis*, eds. A. Sayari and M. Jaroniec, Elsevier, 2005, vol. 156, pp. 401–408.

30 Z. Qin, L. Lakiss, J.-P. Gilson, K. Thomas, J.-M. Goupil, C. Fernandez and V. Valtchev, *Chem. Mater.*, 2013, **25**, 2759–2766.

31 N. S. Nesterenko, F. Thibault-Starzyk, V. Montouilliout, V. V. Yushchenko, C. Fernandez, J.-P. Gilson, F. Fajula and I. I. Ivanova, *Kinet. Catal.*, 2006, **47**, 40–48.

32 R. Jain, A. J. Mallette and J. D. Rimer, *J. Am. Chem. Soc.*, 2021, **143**, 21446–21460.

33 S. Bordiga, P. Ugliengo, A. Damin, C. Lamberti, G. Spoto, A. Zecchina, G. Spanò, R. Buzzoni, L. Dalloro and F. Rivetti, *Topics in Catalysis*, 2001, **15**, 43–52.

34 I. C. Medeiros-Costa, E. Dib, F. Dubray, S. Moldovan, J.-P. Gilson, J.-P. Dath, N. Nesterenko, H. A. Aleksandrov, G. N. Vayssilov and S. Mintova, *Inorg. Chem.*, 2022, **61**, 1418–1425.

35 F. Dubray, E. Dib, I. Medeiros-Costa, C. Aquino, D. Minoux, S. van Daele, N. Nesterenko, J.-P. Gilson and S. Mintova, *Inorg. Chem. Front.*, 2022, **9**, 1125–1133.

36 E. Dib, I. Medeiros Costa, G. N. Vayssilov, H. A. Aleksandrov and S. Mintova, *Journal of Materials Chemistry A*, 2021, **9**, 27347–27352.

37 E. Dib, J. Grand, A. Gedeon, S. Mintova and C. Fernandez, *Microporous and Mesoporous Materials*, 2021, **315**, 110899.

38 A. Beuque, H. Hao, E. Berrier, N. Batalha, A. Sachse, J.-F. Paul and L. Pinard, *Appl. Catal. B: Environ.*, 2022, **309**, 121274.

39 R. W. Borry, Y. H. Kim, A. Huffsmith, J. A. Reimer and E. Iglesia, *J. Phys. Chem. B*, 1999, **103**, 5787–5796.

40 J.-P. Tessonnier, B. Louis, S. Rigolet, M. J. Ledoux and C. Pham-Huu, *Appl. Catal. A: Gen.*, 2008, **336**, 79–88.

41 C. H. L. Tempelman and E. J. M. Hensen, *Appl. Catal. B: Environ.*, 2015, **176–177**, 731–739.

42 N. Kosinov, E. A. Uslamin, F. J. A. G. Coumans, A. S. G. Wijpkema, R. Y. Rohling and E. J. M. Hensen, *ACS Catal.*, 2018, **8**, 8459–8467.

43 F. Thibault-Starzyk, A. Vimont and J.-P. Gilson, *Catal. Today*, 2001, **70**, 227–241.

44 K. Barbera, F. Bonino, S. Bordiga, T. V. W. Janssens and P. Beato, *J. Catal.*, 2011, **280**, 196–205.

45 F. Thibault-Starzyk, A. Vimont, C. Fernandez and J.-P. Gilson, *Chem. Commun.*, 2000, 1003–1004.